View metadata, citation and similar papers at core.ac.uk

brought to you by CORE

provided by Nottingham ePrints

Subcellular calcium dynamics in a whole cell model of an atrial myocyte

Rüdiger Thul [*], **Stephen Coombes** [*], **H. Llewelyn Roderick** [†] [‡], **and Martin D. Bootman** [†]

[*]School of Mathematical Sciences, University of Nottingham, Nottingham, NG7 2RD, UK,[†]Laboratory of Signalling and Cell Fate, The Babraham Institute, Babraham, Cambridge, CB22 3AT, UK, and [‡]Department of Pharmacology, University of Cambridge, Tennis Court Road, CB2 1PD

Submitted to Proceedings of the National Academy of Sciences of the United States of America

In this study, we present an innovative mathematical modelling approach that allows detailed characterisation of Ca^{2+} movement within the 3-dimensional volume of an atrial myocyte. Essential aspects of the model are the geometrically realistic representation of Ca^{2+} release sites and physiological Ca^{2+} flux parameters, coupled with a computationally inexpensive framework. By translating non-linear Ca^{2+} excitability into threshold dynamics, we avoid the computationally demanding time-stepping of the full partial differential equations that are often used to model Ca^{2+} transport. Our approach successfully reproduces key features of atrial myocyte Ca^{2+} signalling observed using confocal imaging. In particular, the model displays the centripetal Ca^{2+} waves that occur within atrial myocytes during excitation-contraction coupling, and the effect of positive inotropic stimulation on the spatial profile of the Ca^{2+} signals. Beyond this validation of the model, our simulation reveals novel observations about the spread of Ca^{2+} within an atrial myocyte. In particular, the model describes the movement of Ca^{2+} between ryanodine receptor (RyR) clusters within a specific z-disk of an atrial myocyte. Furthermore, we demonstrate that altering the strength of Ca^{2+} release, RyR refractoriness, the magnitude of initiating stimulus, or the introduction of stochastic Ca^{2+} channel activity can cause the nucleation of pro-arhythmic travelling Ca^{2+} waves. The model provides clinically-relevant insights into the initiation and propagation of subcellular Ca^{2+} signals that are currently beyond the scope of imaging technology.

atrial myocytes, calcium signalling, computational cell biology

A human heart beats more than a billion times during the average lifespan, and is required to do so with great fidelity. The ventricular chambers of the heart are responsible for generating the force that propels blood to the lungs and body (1). Under sedentary conditions, the atrial chambers make only a minor contribution to blood pumping. However, during periods of increased hemodynamic demand, such as exercise, atrial contraction increases to enhance the amount of blood within the ventricles before they contract. This 'atrial kick' is believed to account for up to 30 % extra blood pumping capacity. Deterioration of atrial myocytes with ageing causes the loss of this blood pumping reserve, thereby increasing frailty in the elderly. Atrial kick is also lost during atrial fibrillation (AF), the most common form of cardiac arrhythmia. The stagnation of blood within the atrial chambers during AF can cause thrombus formation, leading to thromboembolism. Approximately 15 % of all strokes occur in people with AF. As shown in numerous reports, the genesis and maintenance of AF is causally linked to the dysregulation of Ca^{2+} signalling (2–4). Detailed characterisation of Ca^{2+} movement within atrial myocytes is therefore necessary to understand changes involved in ageing and conditions such as AF.

Elevation of the cytosolic Ca^{2+} concentration is the trigger for contraction of cardiac myocytes (1). Engagement of Ca^{2+} with troponin C (TnC) allows the actin and myosin filaments to interact and slide past each other, thereby causing cell shortening. The sequence of events that leads to a Ca^{2+} rise during excitation-contractions coupling (EC-coupling) is well known. Essentially, depolarisation of cardiac myocytes activates voltage-operated Ca^{2+} channels (VOCs) that allow the entry of Ca^{2+} from the extracellular space. This Ca^{2+} influx signal is greatly amplified via a process known as Ca^{2+}-induced Ca^{2+} release (CICR) by intracellular Ca^{2+} channels ('ryanodine receptors'; RyRs) expressed on the sarcoplasmic reticulum (SR). The SR membrane bearing RyRs comes within 10 nm of the sarcolemma, thereby forming compartments known as 'dyadic junctions' in which CICR rapidly occurs. Mammalian ventricular myocytes have an extensive series of sarcolemmal invaginations ('T-tubules') that bring VOCs and RyRs into close proximity within dyadic junctions throughout the volume of the cells. Each dyadic junction produces an elementary Ca^{2+} signal known as a 'Ca^{2+} spark' during EC-coupling. The spatial overlap of many thousands of Ca^{2+} sparks gives rise to the homogenous Ca^{2+} signals associated with ventricular EC-coupling.

In contrast, the atrial myocytes of many mammalian species do not express extensive T-tubule networks. In this situation, the coupling of VOCs and RyRs occurs at dyadic junctions around the periphery of the cells. The consequence of this arrangement is that Ca^{2+} signals originate around the edge of atrial myocytes during EC-coupling (2). We, and others, have shown that under resting conditions this peripheral Ca^{2+} signal does not propagate into the centre of atrial cells, so that at the peak of the response substantial Ca^{2+} gradients can be observed from a cell's edge to its centre (5–7). However, in addition to the junctional RyRs that are activated at the onset of EC-coupling, atrial myocytes express clusters of RyRs in a regular 3-dimensional lattice throughout their volume. It could be expected that these non-junctional RyRs would sense the subsarcolemmal Ca^{2+} signal and convey it deeper into a cell via CICR. Indeed, to trigger substantial contraction, the Ca^{2+} wave must move towards the centre of an atrial cell, since the extent of inward movement of the Ca^{2+} wave and atrial myocyte contraction are linearly related (8, 9). The non-junctional RyRs therefore appear to act as an inotropic reserve that becomes active under conditions where greater atrial contraction is required. Little is known about the mechanisms that control the propagation of Ca^{2+} between RyRs within atrial myocytes.

In the present study, we characterised the movement of Ca^{2+} during EC-coupling in an idealised atrial myocyte model. The model describes a 3-dimensional lattice of discrete Ca^{2+} release sites that equate in position and function to those

Reserved for Publication Footnotes

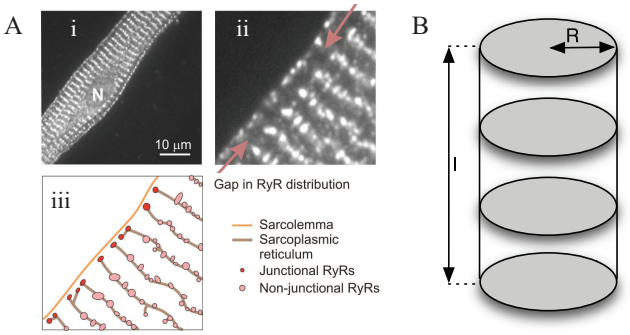

Fig. 1. A: Distribution of type 2 RyRs in an atrial myocyte immunostained with an anti-type 2 RyR antibody. Panel Ai depicts a portion of an atrial myocyte. The transverse striations of non-junctional RyRs, and peripheral junctional RyRs are evident. "N" denotes the position of the nucleus. Panel Aii shows an enlarged section of the same cell. The gap in RyR distribution between the junctional RyRs and the non-junctional RyRs is depicted by the arrows. Panel Aiii shows a cartoon representation of the arrangement of RyRs and cellular membranes relating to panel Aii. The position of the RyR clusters was determined by thresholding the image in panel Aii so that all positive pixels in the background were absent, and then identifying the remaining areas with positive fluorescence. B: Cylindrical atrial myocyte geometry used in simulations showing a stack of z-planes. The location of individual clusters within a disk is illustrated in Fig. 2A.

within an living atrial cell. Our novel method, which translates key properties of cellular Ca^{2+} transport into a framework of significantly low computational overhead, allows the activity of all the discrete Ca^{2+} release sites to be *simultaneously* monitored, and for Ca^{2+} signals to be activated at any particular site(s).

The model was validated by replicating known properties of atrial myocyte Ca^{2+} signalling, such as the centripetal diffusion of Ca^{2+} from the periphery of an atrial myocyte to the cell centre. Moreover, the model allows us to explore factors critical to the fidelity of Ca^{2+} signalling that cannot be manipulated experimentally. Although our simulations utilised the geometry of an atrial myocyte without T-tubules, our findings are also relevant to other myocytes that do not possess T-tubules (e.g. neonatal myocytes). Furthermore, T-tubules in mature ventricular myocytes are lost during ageing or in disease conditions. In situations where T-tubules are lost, EC-coupling is initiated around the periphery of the cells and contraction will be dependent on saltatoric Ca^{2+} wave propagation as for the atrial myocytes described in this study. The arrhythmic calcium wave activity presented herein is relevant to tubulated and non-tubulated myocytes.

Results

The aim of this study was to produce a geometrically realistic model of an atrial myocyte. By incorporating the actual positioning of discrete Ca^{2+} release sites, we could explore their interaction and involvement in Ca^{2+} wave initiation and propagation. Based on empirical measurements of RyR distribution from numerous studies (2) (Fig. 1A), we modelled an atrial myocyte as a cylinder 100 μm in length and 12 μm in diameter, as depicted in Fig. 1B. Within the cylinder, Ca^{2+} release was constrained to 51 2-dimensional disks situated perpendicular to the long axis of the cylinder, and spaced 2 μm apart. These disks correspond to the z-planes within atrial myocytes where the RyRs are expressed (8, 10, 11) (Fig. 1A). Within the z-planes, the Ca^{2+} release sites were distributed as shown in Fig. 2A. The outermost ring of Ca^{2+} release sites represents the junctional RyRs that face the VOCCs in dyadic junctions, whilst the inner Ca^{2+} release sites equate to the non-junctional RyRs. The radial distance between the rings of non-junctional Ca^{2+} release sites is 1 μm (Fig. 2A). Between the junctional Ca^{2+} release sites and the first ring of non-junctional Ca^{2+} release sites is a spacing of 2 μm, reflecting the gap of RyR expression observed in atrial myocytes (Fig. 1Aii). The spacing of Ca^{2+} release sites around each ring is 1 μm. This model allows us to investigate the movement of Ca^{2+} within 1, 2 or 3 dimensions, and to examine interactions between Ca^{2+} release sites within the same, or neighbouring, z-planes.

Deterministic release. Movement of Ca^{2+} within the model relies on saltatory wave propagation involving discrete Ca^{2+} release sites. A 1-dimensional representation of such a wave, obtained analytically, is shown in Fig. 2B (details will be published elsewhere). A centripetal Ca^{2+} wave travels from the periphery to the centre of the cell. The propagation rate and amplitude of the Ca^{2+} wave in the full 3-dimensional cell model both diminish as it moves inwardly. Essentially, Ca^{2+} diffusing between successive release sites has to overcome the continual inhibitory effect of SERCAs, and as the Ca^{2+} signal diminishes it takes longer to initiate Ca^{2+} release at the next RyR cluster. It is already established that RyR activity is regulated by a range of factors including luminal Ca^{2+}, phosphorylation, accessory proteins and accessory factors. To simplify the model, we convolved the effect of these factors in two key parameters — release strength and release threshold. These parameters encompass possible changes in the total Ca^{2+} flux through a cluster of RyRs and RyR sensitivity irrespective of the molecular mechanism. Saltatory wave propagation critically depends on release strength and threshold. If the release strength is too small, or the threshold is too high, then Ca^{2+} waves cannot propagate.

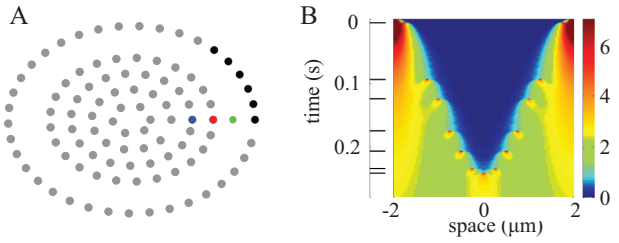

Fig. 2. A: Position of Ca^{2+} release sites within a single z-plane as used in the simulations. See text for details concerning the colours. B: Space-time plot of a 1-dimensional saltatory propagating wave. Parameter values are $\tau = 1\,s^{-1}$, $D = 1\,\mu m^2 s^{-1}$, $c_{th} = 1\,\mu M$ and $\sigma = 0.26\,\mu M$. The bars on the left side indicate the time of successive release Ca^{2+} events

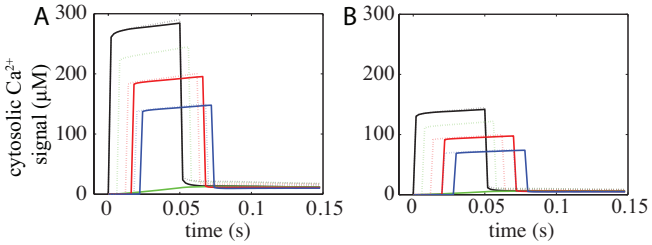

Fig. 3. Time course of the Ca^{2+} concentration for $\sigma = 90\,\mu M\,\mu m^3/s$ (A) and $\sigma = 45\,\mu M\,\mu m^3/s$ (B) in the central z-plane at $\theta = 0$ and $r = 5.9\,\mu m$ (black), $r = 4.9\,\mu m$ (green), $r = 3.9\,\mu m$ (red) and $r = 2.9\,\mu m$ (blue) in the presence (solid line) and absence (dotted line) of a diffusive gap. Parameter values as in Table S1 and $dt = 0.002\,s$.

We next examined the movement of Ca^{2+} within a single z-plane. Ca^{2+} release was initiated by activating the 6 peripheral Ca^{2+} release sites coloured black in Fig. 2A. The black curve in Fig. 3A illustrates the profile of the Ca^{2+} signal at those peripheral sites. The red, blue and green curves depict the time courses of Ca^{2+} concentration at Ca^{2+} release sites deeper inside the cell (denoted by corresponding colours in Fig. 2A). Since we trigger release at the periphery, we observe an immediate response in that location. The next release site (red) opens with some latency, and the peak amplitude is damped in comparison to the outer release site. Moving further towards the interior of the cell, Ca^{2+} release begins even later while peak values continue to decrease. The sharp rise and fall of the concentration profiles is a combined effect of the threshold dynamics of release in a three dimensional volume and the impact of SERCA pumps. Reducing the release strength leads to overall smaller Ca^{2+} profiles and slowing of saltatoric Ca^{2+} wave propagation, but the tendency of growing latencies and smaller maxima for inner release sites remains unchanged (cf. Figs. 3A and 3B). Note that a release strength of $45\,\mu\mathrm{M}\mu\mathrm{m}^3/\mathrm{s}$ corresponds to $\sim$ 400 open RyRs when we assume a single channel current of 1 pA.

An aspect of atrial myocyte ultrastructure that we considered at this point was the effect of the gap in Ca^{2+} release sites between the junctional RyRs and the first ring of non-junctional RyRs. As depicted in 2A, the spacing between rings of Ca^{2+} release sites is $1\,\mu$m inside the cell, with a $2\,\mu$m gap to the peripheral junctional ring of Ca^{2+} release sites. The $2\,\mu$m gap was adopted into the model because studies have shown such a discontinuity in the expression of RyR clusters (10, 12, 13). The physiological reason for this gap in atrial RyR distribution is not known. We observed that for minimal release strengths, the gap prevented the inward propagation of the Ca^{2+} wave, such that only the peripheral Ca^{2+} release sites were active (Fig. S1).

The consequence of incorporating an additional ring of Ca^{2+} release sites (green release site in Fig. 2A) within the gap between the junctional and non-junctional RyRs is depicted in Fig. 3. The essential effect of the additional Ca^{2+} release sites was to accelerate the centripetal propagation of the Ca^{2+} wave by reducing the distance over which Ca^{2+} had to diffuse before attaining a threshold concentration for CICR. These data suggest that the gap in RyR distribution imparts a natural barrier to hinder Ca^{2+} movement. This is likely to be a physiological mechanism for limiting atrial contraction under resting conditions.

The magnitude of atrial myocyte contraction is determined by the distance that the centripetal Ca^{2+} wave is able to spread (2, 8). This is due to the increasing recruitment of myofilaments as Ca^{2+} waves progress deeper into an atrial cell. The extent of propagation of the centripetal wave is modulated by application of positive inotropic hormones such as endothelin-1 or β-adrenergic agonists (8, 14).

To measure the effect of positive inotropic stimulation in our model, we determined the activity of Ca^{2+} release sites within the innermost rings ($r = 0.9\,\mu$m) of all 51 z-planes. For those release sites to be activated, Ca^{2+} has to travel in a saltatoric manner from the periphery of the cell, as described above. We varied the degree of cell stimulation by altering the fraction of peripheral Ca^{2+} release sites that were activated at the inception of a response (hereafter denoted 'initial fraction'; the actual position of those sites was randomly assigned). The black curve in Fig. 4A depicts the increasingly successful recruitment of central Ca^{2+} release sites as the initial fraction was progressively enhanced. The data show that for strong stimulation, i.e. for a large initial fraction, almost all release sites in the innermost rings become activated. On the other hand, a lesser initial fraction elicits a considerably damped response in the centre.

An unexpected outcome was that the variance of central channel opening was not uniform. Generally, triggering either relatively few, or many, peripheral Ca^{2+} release sites gave consistent responses (small error bars on the curves in Fig. 4A. Whereas, activating an intermediate number of peripheral Ca^{2+} release sites gave more variable penetration into the cell (large error bars). The error bars indicate that not all triggered responses, even with the same number of initiating Ca^{2+} release sites, resulted in the same degree of centripetal Ca^{2+} wave propagation. The key point of this observation is that Ca^{2+} waves sometimes propagate into the cell centre, but at other times fail, even though they were triggered by the same number of peripheral release sites. This implies that the positions of the initiating sites is critical. Evidently, some configurations of initial calcium release sites fail to nu-

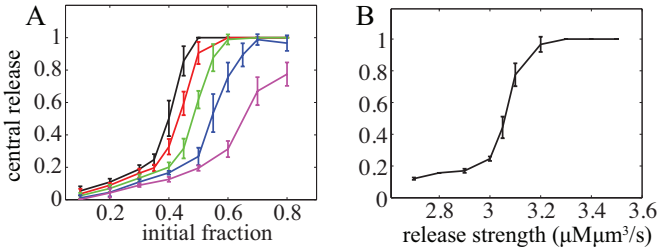

Fig. 4. Mean relative response and variance (error bars) of the central cylinder of release sites ($r = 0.9\,\mu$m) as a function of initial fraction (A) and varying Ca^{2+} release strength σ (B). Parameter values are: (A) $\sigma = 3.5$ (black), 3.4 (red), 3.3 (green), 3.2 (blue), $3.1\,\mu\mathrm{M}\,\mu\mathrm{m}^3/s$ (magenta); (B) initial fraction is 0.8. All other parameter values as in Table S1 and $t_{\mathrm{ref}} = 1$ s.

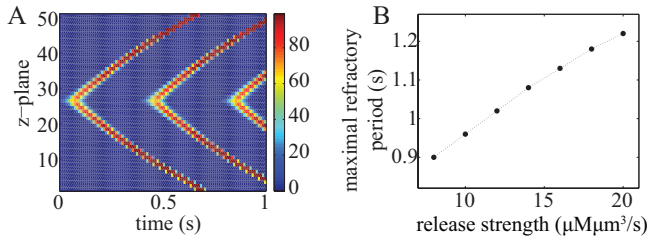

Fig. 5. A: Travelling wave initiated in the central z-plane for $\sigma = 90\,\mu\mathrm{M}\,\mu\mathrm{m}^3/\mathrm{s}$ and $t_{\mathrm{ref}} = 0.34$ s. The Ca^{2+} wave was initiated by activating six adjacent peripheral release sites. B: Maximal refractory period as a function of the release strength σ. a Colours represent the proportion of open channels in a single z-plane.

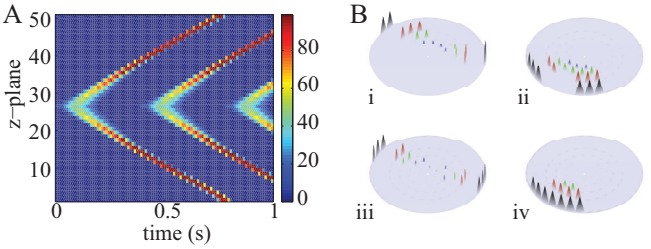

Fig. 6. A: Travelling wave initiated in the central z-plane for $\sigma = 7.85\,\mu\mathrm{M}\,\mu\mathrm{m}^3/\mathrm{s}$ and $t_{\mathrm{ref}} = 0.34$ s. The Ca^{2+} wave was initiated by activating six adjacent peripheral release sites. Colours represent the proportion of open channels in a single z-plane. B Ping wave in the central z-plane at $t = 0.18$ s (i), 0.33 s (ii), 0.60 s (iii) and 0.75 s (iv). The triangular shape of the concentration peaks is for illustration purposes only. Parameter values as in Table S1.

cleate calcium waves. However, the same number of initiating sites, but in a different spatial configuration, can activate a centripetal calcium wave. Interestingly, we have previously observed that atrial myocytes use the same spatial distribution of initiating release sites with each beat (so-called 'eager sites', (13)), thereby avoiding beat-to-beat variability in Ca^{2+} wave nucleation.

Varying the release strength alters the dependency of centripetal Ca^{2+} propagation on the initial fraction (coloured curves in Fig. 4A). Essentially, for lesser release strengths a greater initiating fraction of Ca^{2+} release sites is required to trigger centripetal Ca^{2+} wave propagation. The steep relationship between recruitment of the innermost Ca^{2+} release sites and strength of Ca^{2+} liberation with fixed initial fraction (0.5) is depicted in figure Fig. 4B. In addition to the positive inotropic effects of increased release strength and increased initial fraction, decreasing the threshold for Ca^{2+} release also promoted centripetal Ca^{2+} waves, and would therefore be positively inotropic (Fig. S2). A comparison of the effects of increasing release strength, increasing initial fraction and decreasing threshold is depicted in Fig. S3. It is evident that altering any of the parameters could independently enhance centripetal Ca^{2+} wave propagation, but the effects of each parameter were not exactly alike. Increasing the initial fraction or decreasing the threshold for Ca^{2+} release promoted centripetal Ca^{2+} wave propagation and increased the global amplitude of pacing-evoked Ca^{2+} signals. However, the degree of Ca^{2+} signal enhancement was significantly greater if the Ca^{2+} release strength was increased. Essentially, increasing the release strength is the only parameter that actually adds more Ca^{2+} to the system. The other two parameters, initial fraction and threshold, can modulate the ease with which centripetal Ca^{2+} waves can be triggered and propagate, but do not impart any additional Ca^{2+} inside the cell. These analyses suggest that at least three different parameters control the success of Ca^{2+} wave movement within an atrial myocyte, but that release strength is the most potent effector.

The 3-dimensional atrial cell model also allows us to explore putative arrhythmic patterns of Ca^{2+} signalling that arise from localised Ca^{2+} release activity. In particular, we examined how Ca^{2+} liberated at one z-plane influences Ca^{2+} release sites in neighbouring z-planes. Such a situation is depicted in Fig. 5A, which shows Ca^{2+} waves initiating at the central z-plane within an atrial myocyte that subsequently propagate to the top and bottom of the cell. The figure shows three travelling Ca^{2+} waves of which only the first one was triggered, and the second and third arose autonomously. The reinitiation of such Ca^{2+} waves occurs if the Ca^{2+} concentration within the z-plane that was first triggered is above the threshold for Ca^{2+} release when the RyRs emerge from being refractory. The reinitiation of Ca^{2+} waves reflects an interplay between the processes that serve to introduce Ca^{2+} into the cytoplasm (i.e. Ca^{2+} release strength), the processes that diminish the build-up of Ca^{2+} concentration (i.e. SERCA pumps and Ca^{2+} diffusion) and the refractory period of the Ca^{2+} release sites. Figure 5B depicts the relationship between Ca^{2+} release strength and the maximal refractory period that will sustain Ca^{2+} wave reinitiation. Essentially, as the Ca^{2+} release strength increases, the time window in which Ca^{2+} wave reinitiation can occur also increases. Increasing the time constant of the SERCA pumps and hence weakening Ca^{2+} resequestration also extends the time window for Ca^{2+} waves reinitiation, because it takes longer for the Ca^{2+} concentration to fall below threshold for any given release strength. In addition to increased release strength triggering arrhythmic Ca^{2+} waves, we observed that drammatically decreasing release strength also promoted autonomous Ca^{2+} signals. Below a critical Ca^{2+} release strength, RyR activity persists indefinitely once it is activated within a particular plane. This can be inferred from the faint bluish horizontal ribbon in Fig. 6A. The blue band represents a Ca^{2+} wave that never terminates because the release sites within that plane are never in a simultaneous refractory state. We call this type of activity 'ping waves', and within the model such waves are visualised as an elevated Ca^{2+} concentration within two counter-rotating sectors of a single z-plane (see movie in Supporting Material). These perpetually rotating ping waves progressively feed Ca^{2+} to neighbouring z-planes, eventually evoking longitudinal Ca^{2+} waves. Essentially, a low Ca^{2+} release strength causes only a partial recruitment of Ca^{2+} release sites during EC-coupling, thereby seeding ping wave activity. The period of a ping wave is much longer than the typical time scale for replenishing the SR after Ca^{2+} release, allowing the SR to return to its rest state before a new rotation of a ping wave is initiated. These observations are pertinent to conditions such as end-stage heart failure where Ca^{2+} pumping into the SR is low and RyR expression is diminished (hence release strength is decreased), yet the propensity for arrhythmic Ca^{2+} release is high. The reduced Ca^{2+} release strength evident during heart failure would have the consequence of non-uniform RyR refractoriness, thereby leading to the likely triggering of ping waves.

Stochastic release. In the previous sections, the modelling assumed a uniform threshold for activation of Ca^{2+} release sites. However, ion channels are intrinsically stochastic (15), and within the heart the stochastic activity of RyRs is enhanced by factors such as phosphorylation, association with accessory proteins and increased SR Ca^{2+} load. To model these effects, we make the threshold for Ca^{2+} release a random variable that fluctuates independently at each release site. Figure 7 shows the number of open channels in every z-plane as a function of time and illustrates how Ca^{2+} wave dynamics changes when threshold noise grows. At small noise levels (Fig. 7A), Ca^{2+} wave propagation resembles a deterministic motion, as in Fig. 5. Upon increasing the noise strength, waves emerge spontaneously (Fig. 7B). When two waves meet, they annihilate each other because they run into each other's refractory

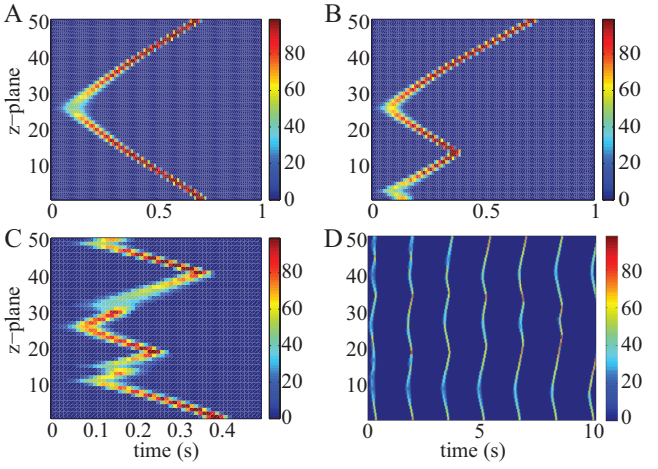

Fig. 7. Travelling wave for $\sigma = 60\,\mu\mathrm{M}\mu\mathrm{m}^3/\mathrm{s}$ and $\beta = 200\,\mu\mathrm{M}^{-1}$ (A), $\beta = 100\,\mu\mathrm{M}^{-1}$ (B), $\beta = 80\,\mu\mathrm{M}^{-1}$ (C) and $\beta = 70\,\mu\mathrm{M}^{-1}$ (D). The first Ca^{2+} wave was initiated by activating six adjacent peripheral release sites. Parameter values as in Table S1 and $t_{\mathrm{ref}} = 1.5\,\mathrm{s}$. Colours represent the proportion of open channels in a single z-plane.

tail. Note that the spontaneously nucleated wave is weaker in the beginning compared to the induced wave, but eventually induces a longitudinal Ca^{2+} wave. Stronger noise leads to more spontaneous waves (Fig. 7C). If the noise strength grows beyond a critical value, almost all channels open immediately. This results in a global rise of activity without any travelling wave.

As described above, refractoriness has a calming influence on Ca^{2+} release by preventing repetitive activation of release sites. A long refractory period ensures that Ca^{2+} declines below the threshold for Ca^{2+} release at the end of a response. However, the introduction of noise can negate the effect of refractory periods on the fidelity of Ca^{2+} signalling. In figure 7D, for example, several successive waves are evident in a simulation using a relatively long refractory period (1.5 s). In the deterministic model with no noise, only the first (triggered) Ca^{2+} wave would be evident. Essentially, introducing noisy thresholds allows some release sites to activate even when Ca^{2+} has recovered to diastolic levels.

Discussion

In the present study we explored the characteristics of Ca^{2+} movement within an idealised atrial myocyte using a realistic geometrical representation of Ca^{2+} release sites and Ca^{2+} flux values. A key feature of the model is that we can initiate Ca^{2+} release from any of the sites within the 3-dimensional lattice, and subsequently examine the propagation of the Ca^{2+} signal to other parts. In this way, we could stimulate the peripheral Ca^{2+} release sites to generate a centripetal Ca^{2+} wave (Figs. 2 and 3) that mimics physiological pacing of atrial myocytes during EC-coupling (6–8, 16), or activate Ca^{2+} release within the centre of the cell to examine the movement of Ca^{2+} waves that would be arrhythmogenic (Figs. 5–7). The propagation of Ca^{2+} signals depends on the diffusion of Ca^{2+} between release sites. If the Ca^{2+} ions released by one site reach the threshold concentration at a neighbouring site, then it will be activated and convey the Ca^{2+} signal further.

Atrial myocytes have an essential inotropic function in the heart. The extent of centripetal propagation of a Ca^{2+} wave determines the extent of atrial myocyte contraction. The further a Ca^{2+} wave progresses towards the centre of the cell, the more myofilaments become activated (5). The junctional Ca^{2+} release sites are always the first to respond during EC-coupling, but by themselves evoke little contraction because the Ca^{2+} signal occurs around the cell periphery. The non-junctional RyRs therefore represent an inotropic reserve that is activated under conditions when strong contraction is required.

A structural feature of atrial myocytes that may credibly contribute to the peripheral restriction of Ca^{2+} waves is the 2 μm gap in RyR expression between the junctional and non-junctional Ca^{2+} release sites (Fig. 1). This gap is a particular feature of atrial myocytes, and has been observed in several previous studies (10, 13). Our results indicate that the 2μm discontinuity in RyR expression significantly hinders the movement of the centripetal Ca^{2+} wave (Fig. 3), because it introduces both a break in the regeneration of the Ca^{2+} wave and a space in which the Ca^{2+} signal can dissipate. Hypothetically introducing Ca^{2+} release sites within the gap has the effects of increasing both the velocity and amplitude of the centripetal Ca^{2+} wave (Fig. 3). These *in silico* results indicate that the gap in RyR expression is a structural feature to prevent inward movement of Ca^{2+}, and thereby reduce atrial energy use when hemodynamic requirements are low.

When hemodynamic demand increases the atrial chambers make a significant contribution to ventricular refilling. Adrenergic stimulation is a key physiological mechanism for enhancing atrial contraction (1) (Fig. S5). The effect of adrenergic stimulation is largely mediated by the activation of protein kinase A (PKA), which has numerous putative targets within a cardiac myocyte. Notably, PKA-dependent phosphorylation causes an increase in VOC activity, which will lead to additional recruitment of dyadic junctions during EC-coupling (analogous to changing the initial fraction). Furthermore, phosphorylation of the endogenous SERCA inhibitor phospholamban causes a marked elevation of SR Ca^{2+} content that both sensitises RyRs for CICR and increases the flux of Ca^{2+} through RyRs upon their activation (analogous to changing threshold and release strength, respectively) (1). It is difficult to experimentally separate the contributions of increased VOC activity, reduced threshold for CICR and increased Ca^{2+} flux. Our simulations indicated that all three parameters have the potential to gradually modulate the inotropic status of an atrial myocyte by determining the ability of centripetal Ca^{2+} waves to propagate from the periphery to the cell centre (Figs. 4 and S3). Furthermore, the effect of these parameters on Ca^{2+} wave propagation was co-dependent. For example, altering the fraction of activated peripheral Ca^{2+} release sites at the onset of a response produced a steeply graded response in terms of centripetal Ca^{2+} wave propagation. Activating only a few of the peripheral Ca^{2+} release sites was generally insufficient to trigger a centripetal Ca^{2+} wave. However, increasing the Ca^{2+} release flux compensated for the lack of peripheral Ca^{2+} release site activation, and promoted centripetal Ca^{2+} waves (Fig. 4). Similarly, decreasing the threshold for CICR, to mimic RyR sensitisation by SR Ca^{2+}, also supported centripetal Ca^{2+} waves. Our data indicates that multiple, interdependent processes determine the ability of centripetal Ca^{2+} waves to propagate, and thereby regulate contraction.

In addition to examining the factors underlying inotropy within atrial myocytes, we explored processes controlling the initiation and propagation of pro-arrhythmic Ca^{2+} waves. As described above, application of adrenergic agonists increases atrial myocyte inotropy, but also leads to the development of spontaneous Ca^{2+} signals (Fig. S4). A plausible explanation for such observations is stochastic activation of RyRs resulting from increased SR Ca^{2+} loading. We modelled this situation by changing the threshold at which cytosolic Ca^{2+} could activate Ca^{2+} release sites randomly in time. It is evident that increasing the spread of thresholds causes progressively more spontaneous Ca^{2+} waves generation (Fig. 7). In addition to RyRs, atrial myocytes express inositol 1,4,5-trisphosphate receptors ($InsP_3Rs$). We and others (2, 5, 14) have demonstrated that specific activation of $InsP_3Rs$ provokes the generation of arrhythmic Ca^{2+} signals. Inclusion of $InsP_3Rs$ within the present model can be mimicked by changing RyR threshold (cf. Fig. 5). Essentially, the stochastic activation of $InsP_3Rs$ triggers further RyR activity and Ca^{2+} waves via CICR. However, even within a deterministic model, where all the Ca^{2+} release sites have the same threshold for CICR, it is possible to trigger self-sustaining autonomous Ca^{2+} waves, such as the Ca^{2+} waves illustrated in Fig. 5. It is evident that several parameters are critical in determining whether autonomous Ca^{2+} waves persist. Essentially, Ca^{2+} waves are triggered when the cytosolic Ca^{2+} concentration is greater than the threshold for CICR. This implies that increased Ca^{2+} release flux or decreased SERCA activity make autonomous Ca^{2+} signals more likely to occur. A further critical parameter determining the propensity for spontaneous Ca^{2+} wave initiation is the period in which RyRs remain refractory af-

ter the previous Ca^{2+} release event (17). Reducing the refractory period increases the likelihood that cytosolic Ca^{2+} will not recover sufficiently before RyRs are ready to respond again (Fig. 5B). Furthermore, mismatches in refractoriness between neighbouring Ca^{2+} release sites can cause the nucleation of Ca^{2+} waves. This is the situation underlying the ping waves presented in Fig. 6, where two counter-rotating Ca^{2+} waves perpetually travel around a z-disk. The ping wave persists because RyRs with the z-disk are never simultaneously refractory. These data therefore suggest that situations in which atrial myocyte Ca^{2+} signalling is enhanced (i.e. increased Ca^{2+} release flux or reduced threshold for CICR) can give rise to pro-arrhythmic Ca^{2+} signals. But, in addition, the activation of RyRs under conditions of relatively weak Ca^{2+} flux also leads to pro-arrhythmic Ca^{2+} release activity due to non-synchronous activation of RyRs and their refractory states.

The formation of ping waves is a clear prediction of our modelling framework, a Ca^{2+} pattern that could not have been resolved with current experimental techniques. Our approach allows us to probe the way in which Ca^{2+} activity between different z-planes interacts, and hence to unravel the complex contributions to physiological and pathological Ca^{2+} signals, which emphasises the useful power of a computational cell biology approach to Ca^{2+} signalling.

Materials and Methods

The dynamics of the Ca^{2+} concentration $c(\mathbf{r},t)$, $\mathbf{r}\in\mathbb{R}^3$, $t\in\mathbb{R}^+$, in the cylinder is governed by a generalisation of the original FDF model (18, 19)

$$\frac{\partial c}{\partial t} = D\Delta c - \frac{c}{\tau} + \sum_{n\in\Gamma}\sum_{m\in\mathbb{N}} \delta\left(\mathbf{r}-\mathbf{r}_n\right)\eta\left(t-T_n^m\right)\,. \qquad \textbf{[1]}$$

Here, D and Δ denote the effective diffusion coefficient for Ca^{2+} and the Laplace operator in cylindrical co-ordinates, respectively. We model sarco-endoplasmic reticulum Ca^{2+} ATPase (SERCA) pumps as homogeneously distributed linear sinks of strength τ. The double sum corresponds to Ca^{2+} liberation from the SR through RyR channels. The $N_{\rm rel}$ release sites are located at discrete positions $\mathbf{r}_n$, $n\in\Gamma=\{1,\ldots,N_{\rm rel}\}$, and $\eta(t)$ holds all details about the release shape, which we here take as $\eta(t)=\sigma\Theta(t)\Theta\left(t-t_{\rm rel}\right)$. Ca^{2+} is released for a fixed time $t_{\rm rel}$ with a constant conductance σ, and $\Theta(x)$ represents the Heaviside step function, which equals 1 for $x\geq 0$ and 0 otherwise. The time T_n^m in Eq. **[1]** corresponds to the instant when the nth release site conducts Ca^{2+} for the mth time. The computation of the release times T_n^m renders Eq. **[1]** highly nonlinear, because the mth liberation is obtained implicitly by demanding that the Ca^{2+} concentration reaches the threshold value $c_{\rm th}$ at time T_n^m and that there is at least a refractory period of $t_{\rm ref}$ between successive release events. When we assume for the moment that all release events occur at multiples of some $\mathrm{d}t$, the concentration profile $c_p\left(\mathbf{r}\right)=c\left(\mathbf{r},p\mathrm{d}t\right)$ is given by

$$c_p\left(\mathbf{r}\right) = \sigma\sum_{n\in\Gamma} a_n(p-1)H\left(\mathbf{r},\mathbf{r}_n,\mathrm{d}t\right) + J_{p-1}(\mathbf{r})\,, \qquad \textbf{[2]}$$

where $H\left(\mathbf{r},\mathbf{r}',t\right)=\int_0^t G\left(\mathbf{r},\mathbf{r}',s\right)\mathrm{d}s$, $a_n(p)$ is a recursively defined indicator function given through

$$a_n(p) = \Theta\left(c_p(\mathbf{r}_n)-c_{\rm th}\right)\prod_{m=1}^{\min(R,p)}\delta\left(a_n(p-m)\right) + \sum_{i=2}^{\min(Q,p)}\Theta\left(c_{\rm th}-c_{p-i+1}(\mathbf{r}_n)\right)\Theta\left(c_{p-i}(\mathbf{r}_n)-c_{\rm th}\right)\,, \qquad \textbf{[3]}$$

and $J_p\left(\mathbf{r}\right)=\int_V G\left(\mathbf{r},\mathbf{r}',\mathrm{d}t\right)c_p\left(\mathbf{r}'\right)\mathrm{d}\mathbf{r}'$. The first term on the right hand side of Eq. **[3]** assures that consecutive release events are separated by at least a refractory period $t_{\rm ref}=R\mathrm{d}t$, while the second term sets the release duration to $t_{\rm rel}=Q\mathrm{d}t$. Note that the functions $H\left(\mathbf{r},\mathbf{r}',t\right)$ need to be computed only once, and the specific form of the Green's function $G\left(\mathbf{r},\mathbf{r}',t\right)$ depends on the boundary conditions. Here we impose finite fluxes across the surface of the cylinder, which mimic e.g. plasma membrane pumps or Na^+/Ca^{2+} exchangers. To investigate the impact of channel noise on wave propagation, we also consider a fluctuating threshold with distribution $f(\xi)$. The random value of the threshold is obtained by the replacement $c_{\rm th}\to c_{\rm th}+\xi$, where ξ is an additive noise term. The indicator function $a_n(p)$ introduced in Eq. **[3]** becomes now a binary random variable, and the probability that $a_n(p)=1$ is obtained from Eq. **[3]** by replacing the first step function Θ by

$$g(\xi) = \left[\frac{1}{1+\mathrm{e}^{-\beta\xi}} - \frac{1}{1+\mathrm{e}^{\beta c_{\rm th}}}\right]\left(1+\mathrm{e}^{-\beta c_{\rm th}}\right)\,, \qquad \textbf{[4]}$$

which relates to the probability distribution f through $g'(\xi)=f(\xi)$. Hence, the stochastic model has the same $t_{\rm rel}$ and $t_{\rm ref}$ as the deterministic one, only the triggering of release is stochastic. The probability of release $P\left(c>c_{\rm th}\right)=g\left(c-c_{\rm th}\right)$ is zero at $c=0$ and tends to one as c becomes large. The strength of the fluctuations is controlled by β, such that larger values of β correspond to a smaller noise strength. In the limit $\beta\to\infty$, the probability $g\left(c-c_{\rm th}\right)$ reduces to the step function $\Theta\left(c-c_{\rm th}\right)$ and we recover the deterministic model. For those simulations mimicking physiological pacing of atrial myocytes, as occurs when an action potential arrives at their sarcolemma, we stimulated Ca^{2+} liberation by activating a proportion of the peripheral Ca^{2+} release sites. Within a single simulated pacing experiment, the proportion of release sites was kept constant, but the position of the activated sites was randomised from pulse to pulse. For a broader and more elaborate discussion of the model, we refer the reader to the section "Model considerations" in the SI.

ACKNOWLEDGMENTS. RT was supported througsh a Leverhulme Trust Early Career Fellowship. MDB and HLR were supported by the BBSRC and BHF. HLR is a Royal Society University Research Fellow.

References

1. Bers, DM (2002) Cardiac excitation-contraction coupling. *Nature*, 415:198–205.
2. Bootman, MD, Smyrnias, I, Thul, R, Coombes, S, Roderick, HL (2011) Atrial cardiomyocyte calcium signalling. *Biochim Biophys Acta*, 1813:922–934.
3. Koivumäki, JT, Korhonen, T, Tavi, P (2011) Impact of sarcoplasmic reticulum calcium release on calcium dynamics and action potential morphology in human atrial myocytes: a computational study. *PLoS Comp Biol*, 7:e1001067.
4. Grandi, E, Pandit, SV, Voigt, N, Workman, AJ, Dobrev, D, Jalife, J, Bers, DM (2011) Human atrial action potential and Ca^{2+} model: Sinus rhythm and chronic atrial fibrillation. *Circ Res*, 109:1055–1006.
5. Mackenzie, L, Bootman, MD, Laine, M, Berridge, MJ, Thuring, J, Holmes, A, Li, WH, Lipp, P (2002) The role of inositol 1,4,5-trisphosphate receptors in Ca^{2+} signalling and the generation of arrhythmias in rat atrial myocytes. *J Physiol*, 541: 395–409.
6. Woo, SH, Cleemann, L, Morad, M (2002) Ca^{2+} current-gated focal and local Ca^{2+} release in rat atrial myocytes: evidence from rapid 2-d confocal imaging. *J Physiol*, 543:439–4532.
7. Sheehan, KA, Blatter, LA (2003) Regulation of junctional and non-junctional sarcoplasmic reticulum calcium release in excitation-contraction coupling in cat atrial myocytes. *J Physiol*, 546: 119–135.
8. Mackenzie, L, Roderick, HL, Berridge, MJ, Conway, SJ, Bootman, MD (2004) The spatial pattern of atrial cardiomyocyte calcium signalling modulates contraction. *J Cell Sci*, 117:6327–6337.
9. Bootman, MD, Higazi, DR, Coombes, S, Roderick, HL (2006) Calcium signalling during excitation-contraction coupling in mammalian atrial myocytes *J Cell Sci*, 119:3915–3925.
10. Carl, SL, Felix, K, Caswell, AH, Brandt, NR, Ball, WJ, Jr, Vaghy, PL, Meissner, G, Ferguson, DG (1995) Immunolocalization of sarcolemmal dihydropyridine receptor and sarcoplasmic reticular triadin and ryanodine receptor in rabbit ventricle and atrium. *J Cell Biol*, 129:673–682.
11. Chen-Izu, Y, McCulle, SL, Ward, CW, Soeller, C, Allen, BM, Rabang, C, Cannell, MB, Balke, CW, Izu, LT (2006) Three-dimensional distribution of ryanodine receptor clusters in cardiac myocytes. *Biophys J*, 91:1–13.

12. Kockskämper, J, Sheehan, KA, Bare, DJ, Lipsius, SL, Mignery, GL, Blatter, LA (2001) Activation and propagation of Ca^{2+} release during excitation-contraction coupling in atrial myocytes. *Biophys J*, 81:2590–2605.
13. Mackenzie, L, Bootman, MD, Berridge, MJ, Lipp, P (2001) Predetermined recruitment of calcium release sites underlies excitation-contraction coupling in rat atrial myocytes. *J Physiol*, 530:417–429.
14. Bootman, MD, Harzheim, D, Smyrnias, I, Conway, SJ, Roderick, HL (2007) Temporal changes in atrial ec-coupling during prolonged stimulation with endothelin-1. *Cell Calcium*, 42: 489–501.
15. Hille B (2001) *Ion Channels of Excitable Membranes*. Sinauer Assoicates, Sunderland, MA USA, 3rd edition.
16. Izu, LT, Means, SA, Shadid, JN, Chen-Izu, Y, Balke, CW (2006) Interplay of ryanodine receptor distribution and calcium dynamics. *Biophys J*, 91:95–112.
17. Niggli, E (2011) Ryanodine receptors: waking up from refractoriness. *Cardiovasc Res* 91:563–564.
18. Keizer, J, Smith, GD, Ponce-Dawson, S, Pearson, JE (1998) Saltatory propagation of Ca^{2+} waves by Ca^{2+} sparks. *Biophys J*, 75:595–600.
19. Coombes, S, Timofeeva, Y (2003) Sparks and waves in a stochastic fire-diffuse-fire model of Ca^{2+} release. *Phys Rev E*, 68:021915.